CMUG CCI+ Deliverable
Number: **D3.1b (5.2.5) Final report**
Submission date: **27 October 2025**
Version: **1.2**

Climate Modelling User Group [CMUG]

Deliverable D3.1b (5.2.5)

Final report

Centres providing input: CMCC (D. Peano, M. Mastropierro), Met Office (D. Hemming, R. King, R. Holliday)

Version nr.	Date	Status
1.0	19 September 2025	First draft shared among partners
1.1	20 October 2025	Internal revision version
1.2	27 October 2025	Submitted to ESA

Deliverable D3.1b (5.2.5)

Final report

Contents

Final report

1. Aim of the deliverable

The WP5.2 study aims to quantify the relationship between changes in plant phenology and land-atmosphere exchanges, with a specific focus on the onset of the growing season. This study uses several Essential Climate Variables (ECVs) to assess their relationships and identify the influence they exert on plant phenology.

The present deliverable provides the main conclusions derived from the results obtained in WP5.2 and perspectives on future developments, which will be part of the optional studies OWP5.2 and OWP5.9. To outline the WP5.2 results, the list of ECVs involved in this study is described in Section 2, the data processing and analysis methodologies are described in Section 3, the results summarised in specific case studies are highlighted in Section 4, and conclusions and outlooks are supplied in Section 5.

2. Essential Climate Variables

The WP5.2 study focuses on vegetation phenology and its relationship with the atmosphere and land conditions. For this reason, various ECVs have been considered in this study, as listed in Table 1.

The principal variable employed in WP5.2 is the Leaf Area Index (LAI), which has been used as a proxy for vegetation phenology, provided by the Vegetation CCI team. Since the LAI has been recently added to the list of ECVs, the first task of WP5.2 (i.e. task 5.2.1) consisted of establishing a direct collaboration between LAI data developers (i.e. CCI Vegetation team) and users (i.e. WP5.2 CMUG team). This activity permitted continuous interactions, feedback, and exchange of information between the two teams, as summarized in CMUG deliverable D2.0bv1 (available from ESA CCI). After the release of the first version of the LAI product, WP5.2 focused on identifying areas of interest by employing the Plant Functional Types (PFTs) distribution map provided by the Land Cover CCI team and the amount of Above Ground Biomass supplied by the Biomass CCI team. Finally, the land surface temperature (LST), provided by the Land Surface Temperature CCI team, and surface and root zone soil moisture (SM), produced by the Soil Moisture CCI team, datasets are used to investigate their interactions with the observed plant phenology. The relationships between LAI, LST, and SM are assessed in the snow-free season, which is identified by means of the snow water equivalent (SWE) variable provided by the Snow CCI team.

Further details on the usage, version, and references of each ECV and feedback on their usability are reported in CMUG deliverable D2.3b (available from ESA CCI).

Table 1: Essential Climate Variables (ECVs), reference Climate Change Initiative (CCI) teams, and release version used in the WP5.2 CMUG study.

CCI Team	Version	Variable
Vegetation	1.0	Leaf Area Index (LAI)
Soil Moisture	9.1	Combined soil moisture, root zone soil moisture
Land Cover	2.0.8	Plant Functional Types distribution
Snow	3.1	Snow water equivalent
Land surface temperature	4.0, 5.11	Land surface temperature
Biomass	5.0.1	Above ground biomass

3. Methodology

3.1 Data pre-processing

The LAI dataset provided by the CCI Vegetation team (referred to as CCI_LAI) offers high temporal and spatial resolutions, 5-day and 1 km, respectively. These characteristics make it suitable for a wide range of applications. However, prior to its use in the present study, the CCI_LAI data must undergo a pre-processing phase. This is to remove values that have high uncertainty, that are anomalous compared to the rest of the time series, and to fill gaps left by these cleaning steps and those gaps already present in the original data. This consists of:

- Quality control based on the flags provided with the dataset;
- Removal of outliers and inconsistent data;
- Gap filling;
- Smoothing of the time series;
- Aggregation to coarser resolutions.

The first quality control step uses the inversion code (invcode) flag provided within the dataset to identify data that is not suitable. This flag provides diagnostics related to the retrieval and inversion performed by the OptiSAIL algorithm (Blessing 2024) and data quality levels (Swinnen et al., 2023; and CMUG deliverable D2.0bv1). It enables filtering of the data according to varying levels of strictness, depending on the requirements of the analysis. Further details and examples are available in CMUG deliverable D2.0bv1 (available from ESA CCI).

Despite applying the strictest quality control options offered by the invcode flag, the resulting dataset still contains outliers, gaps, and inconsistencies. Therefore, additional smoothing and gap-filling procedures are necessary before the data can be used in the WP5.2 study. Notably, the strictest use of the invcode flag also excludes a substantial amount of potentially usable data. This is noted in the product user guide (PUG). For example, in the gridbox at Asa (57.16° N 14.78° E), 41% of time steps are missing after applying this filter, compared to 29% missing in the raw data. This difference is illustrated in Figure 1.

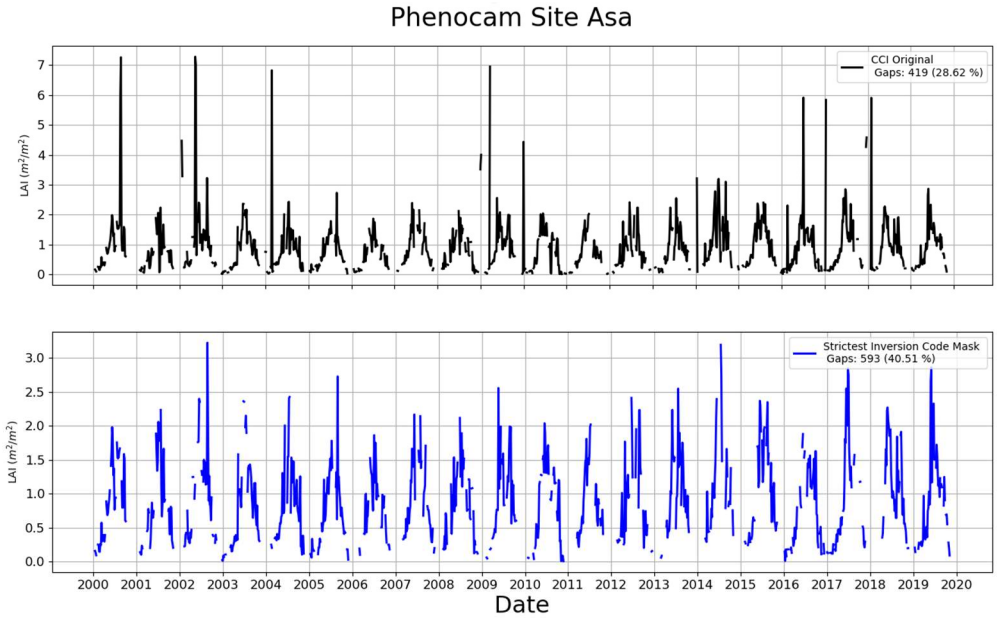

Figure 1: A comparison of before (top, black) and after (bottom, blue) applying the strictest combination of the inversion codes to the CCI_LAI data. At this location, the Phenocam site Asa, there is an increase from 29% to 41% in the number of missing data.

The additional data cleaning phase builds on established approaches from the literature and discussions with the CCI Vegetation team. Figure 2 shows how each of the following steps build up to give the full pre-processing procedure.

Step 1: Filtering by LAI Standard Error

The first step involves using the CCI_LAI standard error provided in the product. Any CCI_LAI value with a standard error greater than one is removed. A large standard error may indicate either poor-quality data returned by the retrieval algorithm, or data that despite being processed without major issues has a level of inherent uncertainty due to limitations in the raw satellite input data. Both cases are undesirable for analysis, making standard error filtering a necessary step. This replaces the use of the invcode to filter data to avoid removing too many potentially good data points. The effect of this filtering is shown in the second row of Figure 2 (green curve).

Step 2: Noise Reduction Using *Z*-Scores

The second step addresses residual noise in the time series using *z*-scores. The *z*-score is a measure of how many standard deviations a data point is away from the mean value. It is calculated for each point in the CCI_LAI time series as:

$$z = \frac{x - \mu}{\sigma} \quad (1)$$

where:

- x is an individual CCI_LAI value,
- μ is the mean of the entire time series,
- σ is the standard deviation of the entire time series,
- z is the resulting *z*-score.

Rather than applying a fixed *z*-score threshold across all sites and grid boxes, which risks being overly strict in low-amplitude regions or too lenient in noisy ones, the 95th percentile of z-scores is computed for each time series. This percentile was chosen empirically. The 90th percentile was tested but found to retain a large number of anomalous values and was therefore rejected. Conversely, using a higher threshold such as the 99th percentile proved too restrictive, particularly in regions with a very short growing season, such as the savannah case study shown in Section 4.3.

The savannah case study highlights a known limitation of this approach where genuinely high LAI values occurring during periods of otherwise low LAI (e.g. from a short rapid onset after a drought-ending storm) may be incorrectly flagged and removed. The combined effect of filtering based on the standard error and then using *z*-scores is shown in the middle row of Figure 2 (purple curve).

An example of where this technique is limited can be seen in Figure 2 - during the winter of 2015 to 2016. Large CCI_LAI values in an otherwise low CCI_LAI period remain visible in the purple curve and persist into subsequent steps.

Step 3: Gap Filling via Linear Interpolation

The third step fills gaps in the time series. This includes data missing from both values absent in the original dataset, and those removed during the previous two filtering steps. Linear regression is applied between valid points on either side of a gap, and interpolated values are inserted at the original time steps. This ensures compatibility with subsequent smoothing functions so they can return a time series with the same original time steps as the CCI_LAI raw data. The fourth row of Figure 2 (red curve) shows the gap-filled time series.

This step is used to fill gaps of any length. Climatology was not chosen to fill long gaps to avoid potentially using low quality data to create the climatological values. The use of climatology would also assume the growing seasons are similar each year. An aim of this work is to investigate if indicators of the growing season are similar or different year-on-year, hence rejecting the use of climatology.

Step 4: Smoothing with the Savitzky-Golay Filter

Although the time series is now temporally complete, residual noise and anomalies may still be present. To address this, the Savitzky-Golay filter is applied, a method commonly used in LAI product processing (e.g. Copernicus Global Land Operations LAI product Verger et al. 2015, 2019). This filter requires two parameters:

1. **Polynomial order.** A third-order polynomial is selected to capture seasonal and sub-seasonal dynamics without introducing additional noise.
2. **Window width.** A window size of 19 time steps is used, corresponding to a 95-day span. This captures a substantial portion of the seasonal cycle while preserving the shorter-term features. This was determined empirically.

The filter is applied once, without any iteration. After applying these four steps, the CCI_LAI data becomes a continuous, smoothed time series. The final result is shown in the bottom panel of Figure 2 (orange curve).

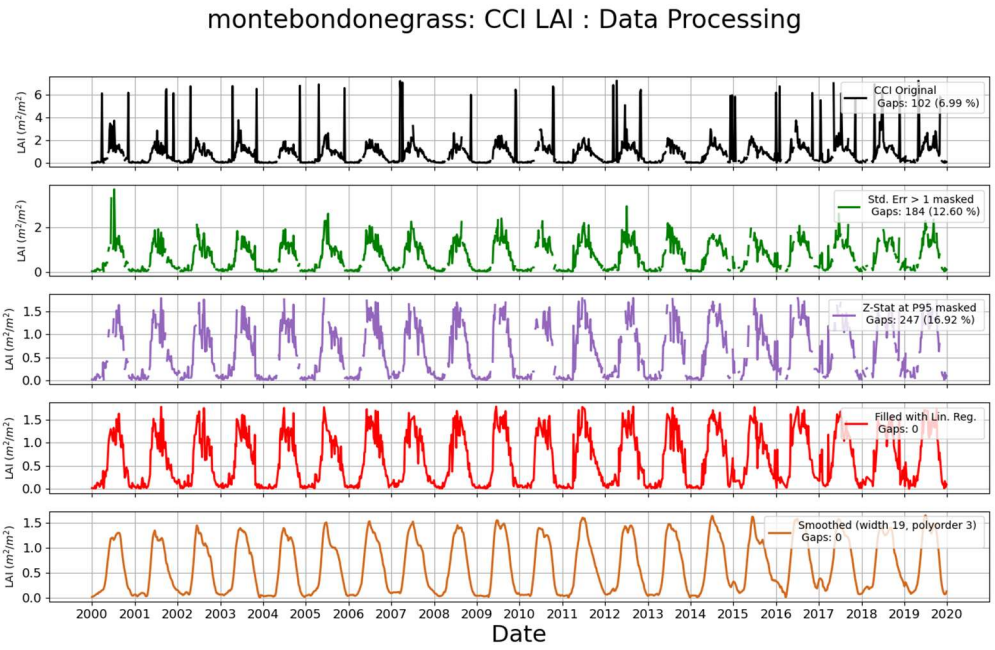

Figure 2: Processing chain applied to CCI_LAI data to prepare it for phenology metric calculations, shown for a single gridbox at Monte Bondone. (Top, black line) Raw CCI_LAI data is first filtered using the standard error (second line, green), then further noise is reduced using a z-score filter (middle, purple line). Gaps are filled using linear regression (penultimate line, red), and the time series is finally smoothed using a Savitzky-Golay filter (bottom, orange).

An alternative method for handling noisy data with gaps was also considered, particularly for detecting the vegetation onset dates. This approach involved fitting a cubic polynomial to the CCI_LAI time series. This is robust to short gaps and moderate noise, especially if the early part of the year contains usable values. However, it still required the prior removal of large anomalies, such as those present in the black curves (the raw CCI_LAI data) of Figure 1 and Figure 2.

The cubic polynomial method was applied on a year-by-year basis, fitting a cubic polynomial from January 1st to the date of maximum CCI_LAI within each year. This provided a smooth representation of the early growing season. Similarly, a second cubic polynomial was fitted from the date of maximum CCI_LAI to December 31st, enabling detection of the end-of-season (offset) using an analogous approach to onset detection.

A key limitation of this approach is the need to fit two separate curves to each annual cycle. This introduces a discontinuity where the first cubic polynomial (typically increasing) meets the second cubic polynomial (typically decreasing). This discontinuity means the method can fail to capture important features such as two growing seasons, the vegetation dynamics changing around the peak of the growing season, and other inter-annual variations where distinct polynomials from consecutive years meet. The discontinuity between the two fitted segments reduces the overall smoothness and may not be representative of real or modelled vegetation.

In scientific analysis, LAI data are correlated and assessed against data and variables from multiple sources which may differ in spatial resolution. To facilitate such comparisons, this final pre-processing step involves aggregating the CCI_LAI data to coarser resolutions. The aggregation methodology incorporates the uncertainty information provided within the dataset. In particular, the relative error (i.e. the ratio between standard error and CCI_LAI value) is used to compute a weighted average (Figure 3), as follows:

$$LAI_{agg} = \frac{\sum_i \left(\frac{LAI_i}{LAI_{re,i}^2} \right)}{\sum_i \left(\frac{1}{LAI_{re,i}^2} \right)} \qquad (2)$$

where:

- i indexes each grid point within the aggregation domain,
- LAI_i is the CCI_LAI value at grid point i,
- $LAI_{re,i}$ is the relative error associated with grid point i,
- LAI_{agg} is the aggregated CCI_LAI value.

This approach means the grid points with lower uncertainty contribute more strongly to the aggregated value. Further details of the methodology are provided in CMUG deliverable D2.0bv1 (available from ESA CCI).

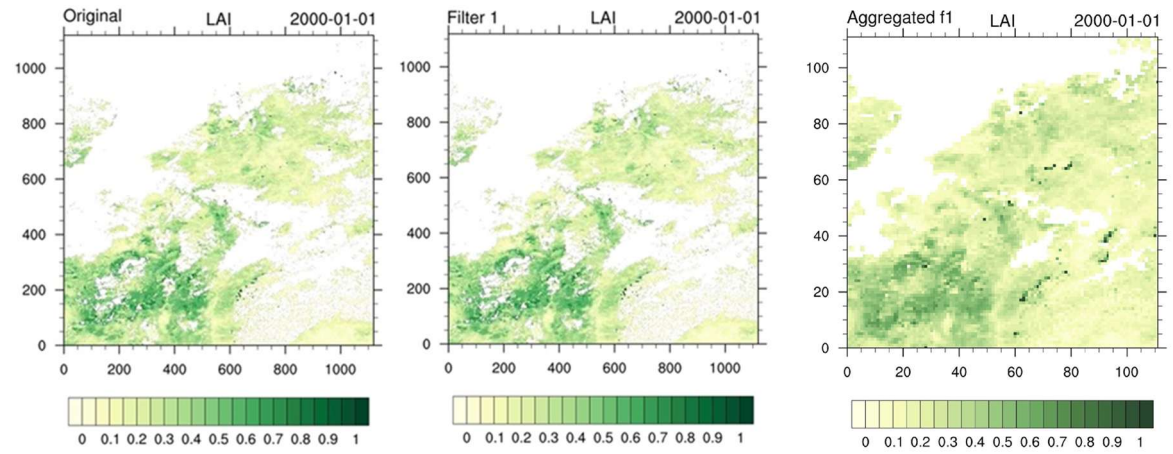

Figure 3. Aggregation of CCI_LAI data. The original data (left) are filtered with the first filter (middle) and aggregated (right) from the original ~1km to ~10km resolution using Equation 2.

3.2 Detection of the onset of the growing season

Recent studies (e.g. Peano et al., 2021, 2025; Li et al., 2022) show that state-of-the-art land surface models (LSMs) simulate a delay in several phenophases, such as start, peak, and end of the vegetative active season. These results highlight a generalised delay of the plant growing season in LSMs. Since this delay occurs from the onset onward, WP5.2 focuses on assessing the main relationships between the onset of the vegetative active season and soil and atmosphere conditions.

To perform this evaluation, the onset is identified by employing the LAI as a proxy of plant phenology. This choice is derived from the availability of LAI as a prognostic variable in LSMs (e.g. Murray-Tortarolo et al., 2013; Peano et al., 2019).

The onset of the growing season is detected by applying the Four Growing Season Types (4GST) methodology (Peano et al., 2019) on the smoothed and gap-filled CCI_LAI data resulting from the pre-processing procedure presented in Section 3.1.

The 4GST methodology identifies the main phenophases at global scales, accounting for four different phenology types:

1. Evergreen;
2. Single growing season, peaking in summer;
3. Single growing season with summer dormancy;
4. Two growing seasons.

Each of these types presents different features and phenophase detection algorithms.

In particular:

1. No phenophase is identified in evergreen areas.
2. In regions with a single growing season, phenophases are detected based on a critical threshold applied to the LAI annual cycle.

3. The same threshold-based approach is used in areas with two growing seasons, but only after separating the two active vegetative periods.

Further details of the method are provided in Peano et al. (2019).

The onset timings detected using the 4GST technique are sensitive to the selected LAI thresholds. To determine appropriate threshold values, the 4GST results are compared against in-situ observations from PhenoCam images (Richardson 2023). Specifically, the threshold values of 20%, 25% and 30% of the annual LAI amplitude are used. These are compared to the onset dates derived from the green chromatic coordinate (GCC) values obtained from the PhenoCam site.

This is illustrated in Figure 4 for a PhenoCam site at Monte Bondone (Northern Italy) which shows a comparison of onset dates calculated from GCC and CCI_LAI at the 20% threshold. Table 2 presents onset dates derived from three threshold levels, 20%, 25% and 30% of the annual CCI_LAI amplitude. To avoid false detection, the onset calculation includes a check for local minima and maxima, ensuring only valid transitions are considered. An example of where this correction is necessary can be seen in Figure 4 where the CCI_LAI has a local maximum in the winter of 2016 into 2017.

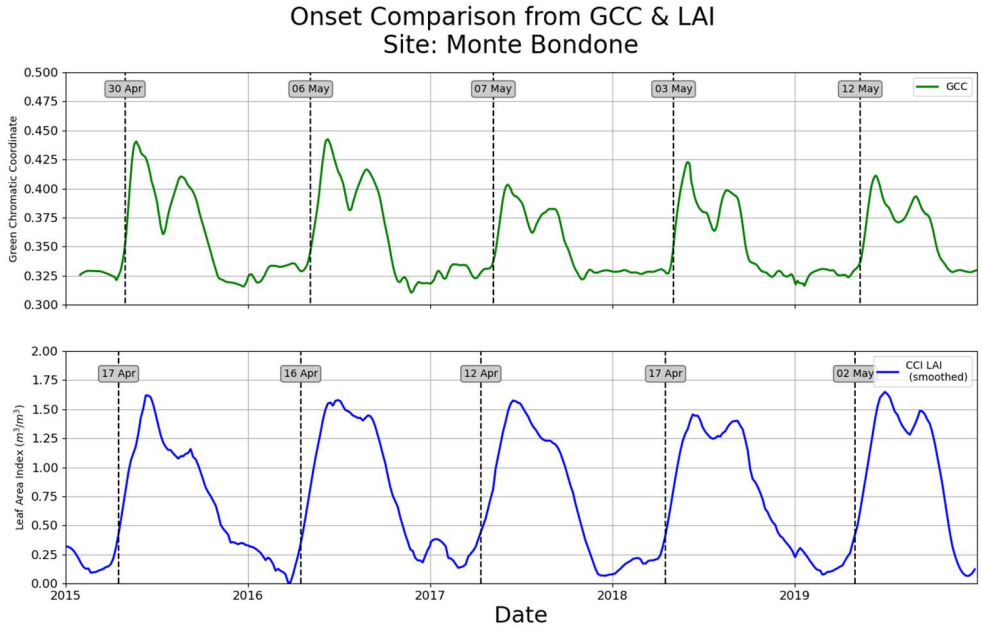

Figure 4: Comparison of vegetation onset dates detected using the Four Growing Season Types (4GST) method: (top, green) based on Green Chromatic Coordinate (GCC), and (bottom, blue) based on CCI Leaf Area Index (CCI_LAI). A threshold of 20% is used in both cases. The data is from the PhenoCam site at Monte Bondone, which is characterised by grassland vegetation.

Table 2: The dates of onset at Monte Bondone calculated from Green Chromatic Coordinate (GCC) and CCI Leaf Area Index (CCI_LAI). Three dates are shown from each year

corresponding to the three threshold levels used, 20%, 25% and 30% of the annual GCC/LAI amplitude.

Year	Onset Date from Green Chromatic Coordinate	Onset Date from Leaf Area Index	Threshold
2015	30 April	17 April	20%
	1 May	22 April	25%
	3 May	27 April	30%
2016	6 May	16 April	20%
	9 May	21 April	25%
	11 May	26 April	30%
2017	7 May	12 April	20%
	10 May	17 April	25%
	12 May	27 April	30%
2018	3 May	17 April	20%
	4 May	22 April	25%
	5 May	22 April	30%
2019	12 May	2 May	20%
	15 May	7 May	25%
	17 May	12 May	30%

It is seen that for the same threshold level, onset dates derived from CCI_LAI are approximately two weeks earlier than those calculated from GCC. This represents 2-3 timesteps (of 5 days) in the CCI_LAI data, which is coarser than the daily GCC. Part of this two-week discrepancy may be attributed to the differing temporal resolutions and sensitivities of the two datasets. LAI is also representative of a whole gridbox (1 km by 1 km for CCI_LAI) compared to GCC being calculated for a small region in the camera's field of view. The difference in spatial scales the data is created over could also explain the difference in onset dates.

The comparison demonstrates that the 4GST method for onset detection gives consistent results when applied to different input variables. Given the distinct properties of LAI and GCC, it is possible that different threshold values may be required to make accurate comparisons. This means that the PhenoCam sites can be used to evaluate threshold and methods developed from this study across their wide range of vegetation type coverage, especially with the next release of the CCI LAI data which will have global coverage.

3.3 Phenology and land-atmosphere conditions

Phenophases and land-atmosphere conditions are often linked through threshold-based and accumulation approaches, such as the Growing Degree Day (GDD) method (e.g. Woodward 1987; White et al., 1997). State-of-the-art land surface models commonly use GDD for computing the relationship between phenology and temperature (e.g. Clark et al., 2011; Lawrence et al., 2019). The same approach is used in this study to estimate the relationship between LST and CCI_LAI, Equation 3,

$$GDD_{sum}^{n} = \begin{cases} GDD_{sum}^{n-1} + \alpha f_{day} & for\ var > threshold \\ GDD_{sum}^{n-1} & for\ var < threshold \end{cases} \quad (3)$$

where:

- GDD_{sum}^{n} is the accumulated GDD at timestep n,
- α is a scaling factor representing how far the variable exceeds the threshold,
- f_{day} is the daily increment to the summation,
- *var* refers to the input variable, LST in this case,
- *threshold* may be constant or vary depending on the species and local climate conditions.

Growing Degree Days are traditionally calculated using near-surface air temperature, particularly in pest modelling and agricultural applications. The limited spatial coverage of in-situ air temperature observations restricts their applicability across large regions or at global scale unless modelled air temperatures are used, such as those from ERA5. Satellite-derived LST observations offer a potential solution with global coverage and daily observations.

It is important to note that LST and near-surface air temperature are distinct physical quantities. LST represents the skin temperature of the Earth's surface, which can differ significantly from the near-surface air temperature typically measured at screen height or at 2 meters from the ground. Despite the two quantities being related, they can differ significantly due to influences such as land cover, vegetation fraction and type, elevation, and time of day (e.g. Good (2016)). LST and near-surface air temperature can diverge significantly due to solar heating and surface properties. As a result, it is expected that LST-based thresholds for GDD calculations will be different to air temperature-based thresholds.

Using a single daily value of LST to calculate GDD risks introducing sampling biases. Infrared (IR) LST measurements from sensors such as the Moderate-Resolution Imaging Spectro-radiometer (MODIS) on Aqua and Terra may be unavailable due to cloud cover, and a single overpass cannot capture the full diurnal temperature range. The details of the diurnal cycle are still not captured when using both the daytime and nighttime overpass observations given in the CCI LST product. Ideally multiple observations per day are needed to estimate both the minimum and maximum LST values. Sub-daily products are available from the CCI LST, combining multiple IR sensors to give a 3 hourly product. However, they do not fully mitigate the sampling issue, for example if the only observations on a particular day are from nighttime overpasses, they may be incorrectly used to estimate the daily maximum.

Microwave (MW) LST products offer all-sky observations, making them valuable for filling gaps caused by cloud cover in IR datasets, or in place of them. However, they do have a lower spatial resolution compared to IR LST products. In this study. combining two CCI LST MW products is used to provide multiple observations per day:

- **SSM/I and SSMIS** Special Sensor Microwave - Imager, and Special Sensor Microwave - Imager/Sounder
- **AMSR-E and AMSR2** Advanced Microwave Scanning Radiometer for EOS, and Advanced Microwave Scanning Radiometer - 2.

Each sensor provides a daily ascending and descending overpass, so combining both products gives up to four observations per day. This allows a value for the daily maximum and minimum LST to be estimated. In version 5.11 of these MW LST products, there is no data available for the year 2012, but all other years in 2003-2019 inclusive are available.

Having estimates for both daily minimum and maximum LST values enables the use of the GDD method described in Baker (1980) and Anon. (1969). For a given day, let the daily minimum and maximum LST values be T_{min} and T_{max} respectively, and a given threshold value be T_0. The daily contribution to GDD, C_d , is calculated as:

1. If $T_{max} \leq T0$, $C_d = 0$,
2. If $T_{min} \geq T0$, $C_d = 0.5*(T_{min} + T_{max}) - T_0$,
3. There are two cases for when T_0 lies between T_{min} and T_{max}:
    a. If $0.5*(T_{min} + T_{max}) > T_0$, $C_d = 0.5*(T_{max} - T_0) - 0.25*(T_0 - T_{min})$,
    b. If $0.5*(T_{min} + T_{max}) < T_0$, $C_d = 0.25*(T_{max} - T_0)$.

Each day's C_d values are summed to a given date to compute the cumulative GDD from MW LST. The values from this algorithm are conceptually similar to the use of α and f_{day} in Equation 2, which exploits the Community Land Model (CLM) internal 30 minute timestep.

The relationship between soil moisture and phenology can also be parametrised using a GDD-like scheme, as implemented in models such as the Community Land Model (e.g. Lawrence et al., 2019). However, the definition of soil moisture thresholds is strongly related to the model's water content parameterisation. This limits the applicability of GDD in linking soil moisture and phenology.

For this reason, the detection of vegetation onset based on soil moisture conditions is derived using an approach that accounts for a (site-specific) standardized amount of volumetric soil moisture (SASM), allowing the application of this method to models that have different soil water content parameterisations. Specifically, phenology onset is detected based on a threshold exceedance approach applied to both a 5-days standardized running mean, and a 30-days standardized running mean of volumetric soil moisture (Equation 4). This approach is conceptually like the one reported in Harris et al., (2025) for flash flood detection, and is justified by the need to simulate phenology onset (and vegetation dynamics more generally) by means of both long-term water availability and short-term soil moisture accumulation (Good et al., 2017).

$$\text{SASM} = \begin{cases} 1, & \text{if } SM_{5d} > \text{threshold}_{5d} \text{ and } SM_{30d} > \text{threshold}_{30d} \\ 0, & \text{otherwise} \end{cases} \qquad (4)$$

where, if both the conditions for long-term (30-days) and short-term (5-days) standardized soil moisture amounts are met, phenology onset is predicted. For the Savannah case study, the thresholds for both the short-term and long-term standardized soil moisture (1.2 and 0.4, respectively) have been optimized to fit the yearly phenology onset as represented by CCI_LAI and estimated by the SASM methodology.

Finally, the climatology annual cycle of temperature and soil moisture, combined with correlations and time lag calculations between these variables and the CCI_LAI timeseries, can be used to identify regions where temperature acts as the main phenology stress factor versus areas where soil moisture is the principal driver of phenology. A mixture of temperature-driven and water-driven phenology will characterise some areas.

Three specific features are required to identify water-driven regions, which are:

- Minimum soil moisture below 0.1 m^3m^{-3} and below 50% the annual range of soil moisture variability.
- Positive correlation between soil moisture and CCI_LAI.
- A positive time-lag correlation between soil moisture and CCI_LAI of a maximum of 30 days.

Similarly, the temperature-driven areas are characterized by:

- Minimum annual temperature below 0 ºC.
- Positive correlation between LST and CCI_LAI.
- A positive time-lag correlation between LST and CCI_LAI of a maximum of 30 days.

4. Case studies

4.1 Detection of water-driven and temperature-driven phenology areas

Based on the local features and correlation of LST, SM, and CCI_LAI, it is possible to identify regions where water or temperature is the principal driver of plant phenology (Section 3.3). The application of the specific criteria described in Section 3.3 provides a procedure to establish the main drivers in each region and areas without a single driver (Figures 5-7).

Since three criteria have been proposed for both temperature-driven and water-driven, it is possible to provide various levels of strictness in the regional selection. The default selection requires that at least two out of three criteria are matched to be listed among one of the two regional categories. The latitudinal transects representing the three criteria for the water-limited and temperature-limited regions are provided in Figures 5 and 6, respectively.
It is therefore possible to identify regions with water-driven or temperature-driven vegetation phenology where either the criteria 2 or 3 are met, and at the same time, the first criterion is met (c1 AND (c2 OR c3)).

The areas presented in Figure 5 and as red pixels in Figure 7a for the soil moisture driven regions resemble what are commonly regarded as semi-arid biomes, despite some regions presenting artefacts due to the inherent limitation of our approach. The Sahel area and the regions south of the equator are indeed classified as soil-moisture driven, whereas the tropical Congo basin forests and European biomes are excluded due to the stronger control of radiation, and both radiation and temperature modulation, respectively. Additionally, parts of the Sahara Desert are excluded, most likely due to their very low minimum and maximum CCI_LAI signals (not shown), which prevent the calculation of reliable correlation and lag-correlation metrics. Lastly, some small areas in Europe, most remarkably in Scandinavia, are classified as soil moisture driven as a direct consequence of their annual soil moisture minimum and amplitude (Figure 5a). This, however, is likely an artificial feature deriving from the usage of the SM-

GAPFILLED dataset, which suffers from the snow-masking effect during the boreal winter in northern latitude regions.

Similarly, the identification of temperature-limited areas derives from the combination of the three proposed criteria (Figure 6). The resulting classified regions are presented as blue pixels in Figure 7b below and are broadly complementary to the water-limited regions in Figure 7a. Overall, the geographical areas in which the phenological seasonality is commonly regarded as temperature (and radiation) driven are correctly classified. These areas substantially embrace the spatial domain north of the Mediterranean sea, characterized mainly by temperate and boreal climatic conditions, with some additional areas in South Africa which experience similar continental climatic conditions. Like in the case of the soil moisture dataset, some notable gaps are found in Scandinavia likely due to missing surface temperature data in some years. Additionally, some artifacts are observed in the Sahara desert regions, in this case as a result of the almost entirely absence of vegetation cover.

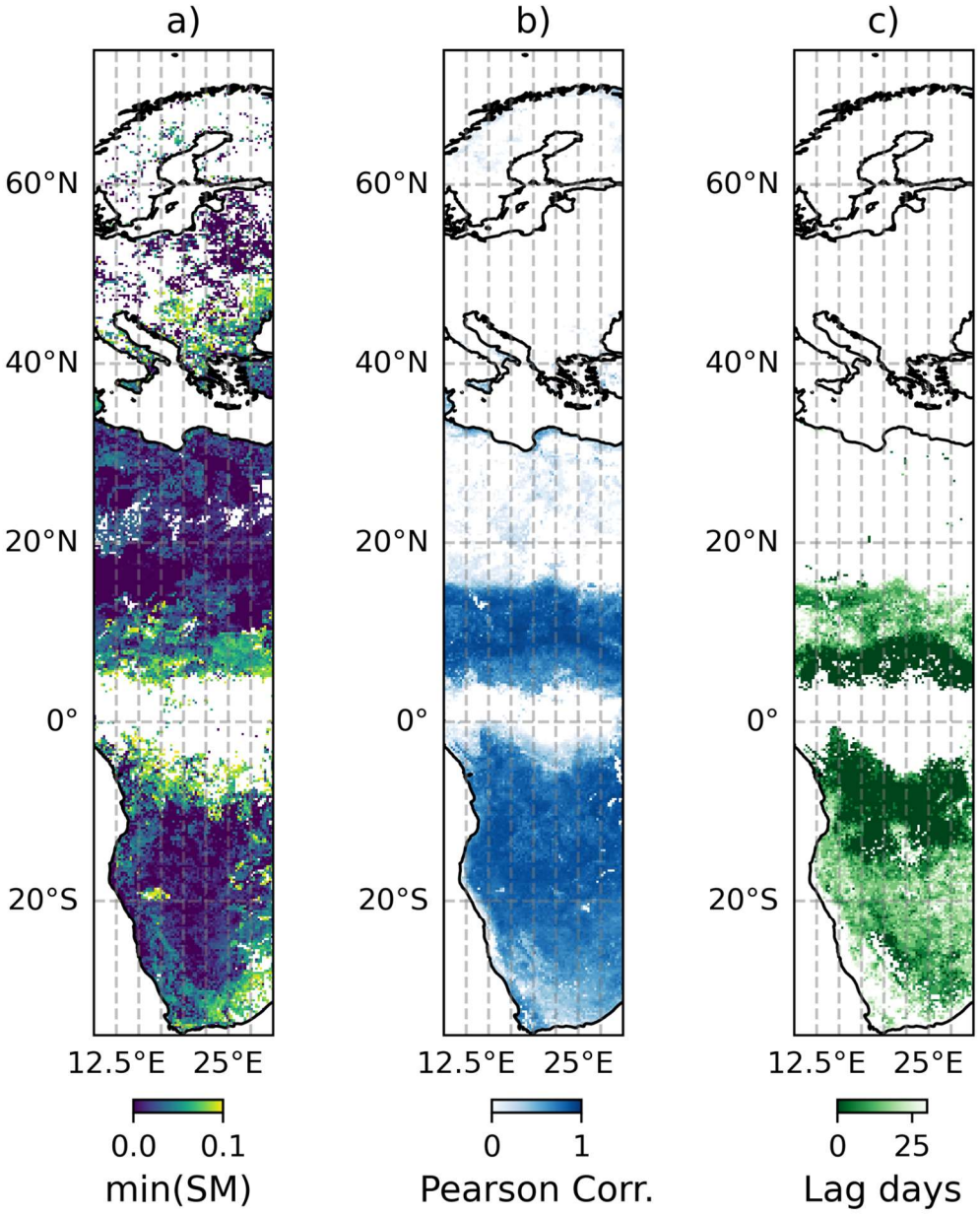

Figure 5: Transect map with soil moisture-limited criteria. Panel a) shows the average annual soil moisture minimum for the pixels that met the first criteria. Panel b) shows the Pearson correlation for the pixels that meet the second criteria. Panel c) shows the maximum lag-correlation for those pixels that meet the third criteria.

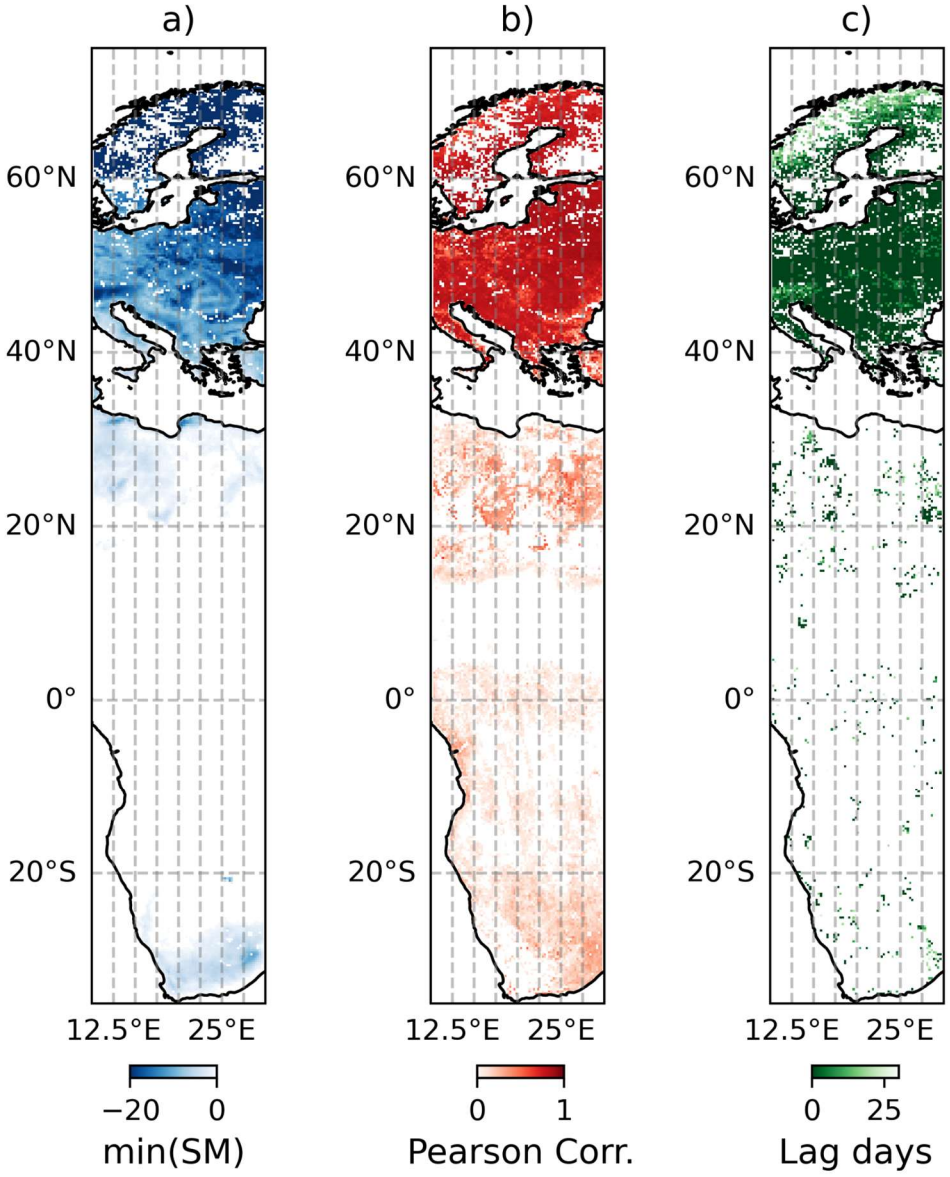

Figure 6: Transect map with temperature-limited criteria. Panel a) shows the climatological minimum annual surface temperature for the pixels that met the first criteria. Panel b) shows the Pearson correlation for the pixels that meet the second criteria. Panel c) shows the maximum lag-correlation for those pixels that meet the third criteria.

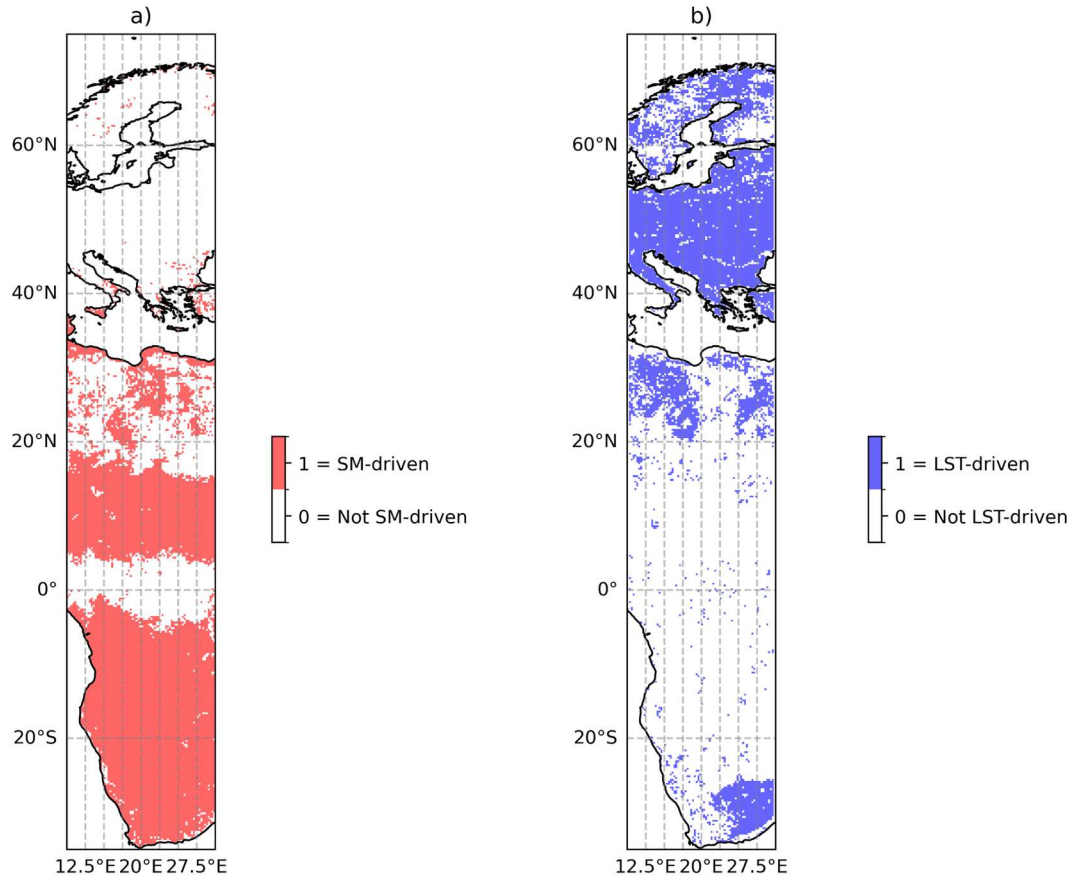

Figure 7: Transect map showing the regions of a) water driven and b) temperature driven vegetation phenology. These regions consist of the areas where two out of the three criteria defined in Section 3.3 are met.

In the following sections, a site-specific case study is performed at Monte Bondone (46.01ºN 11.05ºE) and for a Savannah biome in Chad (14.5°N 22°E), which lies in the temperature and soil moisture driven geographical regions, respectively. Section 4.2 and 4.3 therefore explore the relationship between vegetation onset dates, LST and SM to aid refining the criteria and expand further the analysis.

4.2 Temperature-driven case: Monte Bondone

The Monte Bondone PhenoCam site falls within the spatial coverage of the CCI_LAI dataset. Monte Bondone is suspected to lie within a temperature-driven phenological region. It is selected as a case study to evaluate the relationship between the onset of the growing season, as detected using the 4GST approach applied to CCI_LAI data, and the same phenophase retrieved using the GDD approach applied to MW LST data. This comparison is illustrated in Figures 8 and 10.

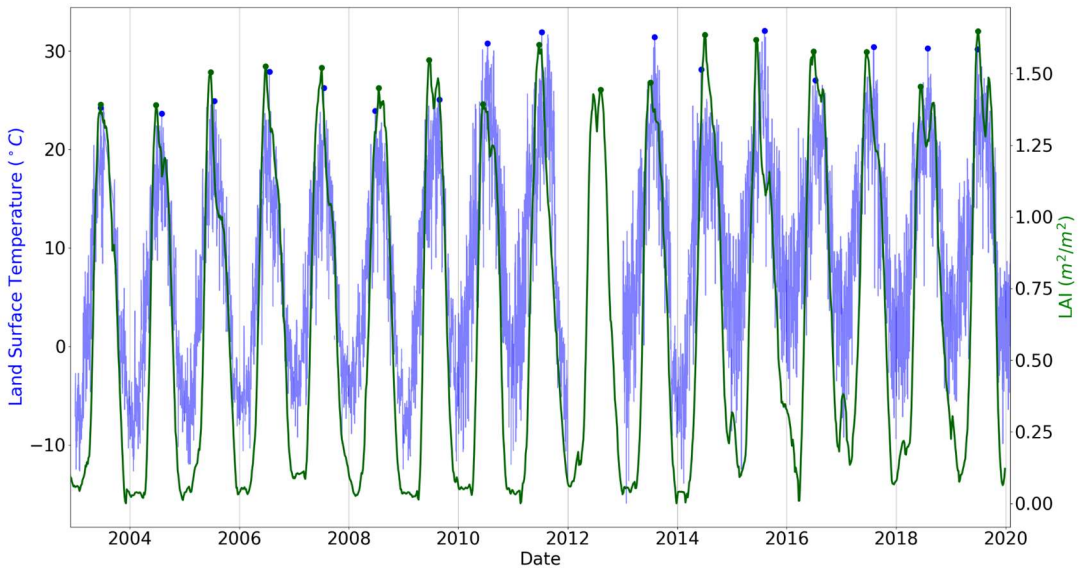

Figure 8: The Land Surface Temperature (LST) in blue and CCI Leaf Area Index (CCI_LAI) in green for the Monte Bondone grassland site. The LST is the maximum of the four values for each day. The blue and green markers show the maximum in each year of the LST and CCI_LAI respectively. There is no LST data available for 2012 in the CCI MW LST products.

The Monte Bondne site shows extended periods each year from 2003 to 2019 during which the maximum daily LST remains below 0ºC, supporting the possibility that phenology at this location is temperature driven, Figure 8. This is further investigated by comparing the dates of the peak LST and peak CCI_LAI, Figure 9. The peak LST date is defined as the day of the year with the highest daily maximum value among the four daily MW LST observations.

At Monte Bondone, a weak linear relationship is observed between the day of the year of peak LST and the day of the year of peak CCI_LAI (R = -0.5, Figure 9). This relationship is affected by the presence of the double peak in CCI_LAI value. The double peak is visible in PhenoCam imagery and is supported by the GCC data shown in Figure 4. In most years, the first CCI_LAI peak is the highest value.

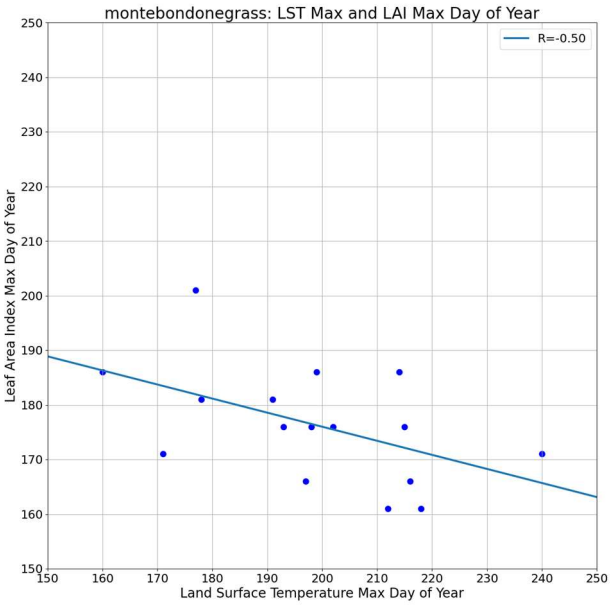

Figure 9: A comparison of the day of the year the maximum value of Land Surface Temperature and Leaf Area Index occurs at the Monte Bondone grass site. The linear regression fit to these points has R = –0.5.

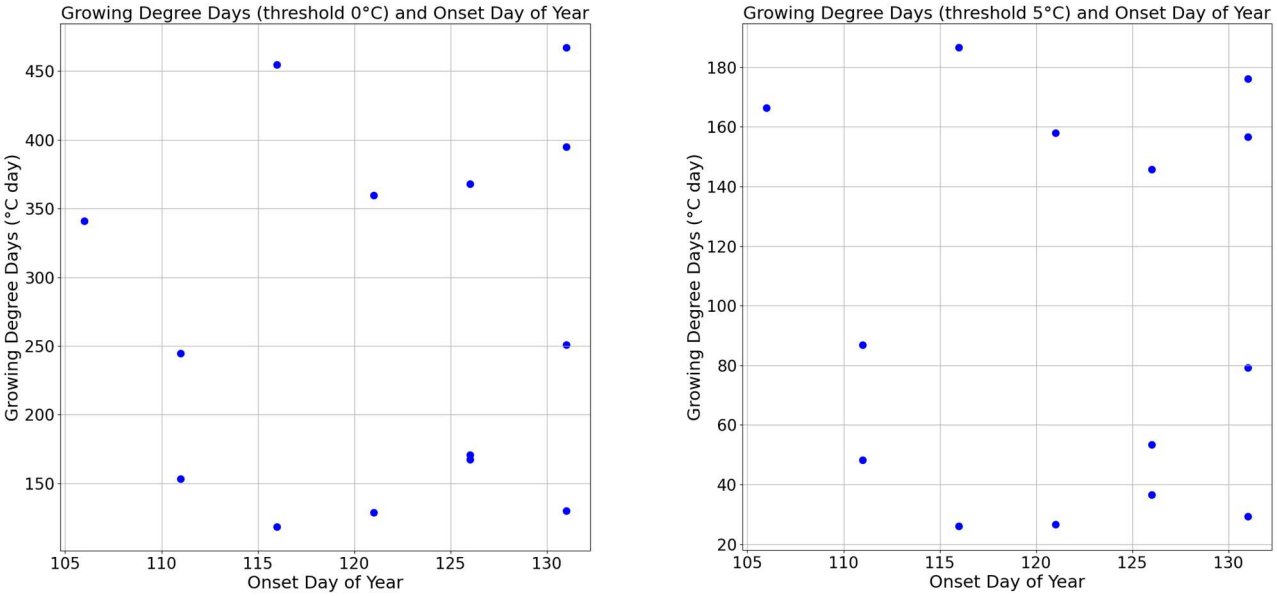

Figure 10: A comparison of the day of the year of onset and the accumulated growing degree days on that day, at the Monte Bondone grass site. (Left) The threshold for the growing degree days is 0°C. (Right) The threshold for the growing degree days is 5°C.

Growing Degree Day values are calculated from 1st January of each year to the detected onset date. These values are computed for two temperature threshold values, 0ºC and 5ºC. The comparison is shown in Figure 10. In this case, there are two distinct modes of behaviour, a range of data where GDD is less than 300 ºCday, and where GDD is greater than 300 ºCday (for a threshold of 0ºC). This bimodal behaviour is explored below. The GDD and onset comparison can show different behaviours corresponding to different climate and biome effects. Figure 11 shows the equivalent plot of Figure 10 for a site at Rosalia (47.7º N 16.3º E). Rosalia is predominantly a needleleaf tree site (85% coverage from CCI Land Cover data) with natural grasses making up the rest of the coverage. A single mode is evident centered around an onset day of the year of day ~100, with a large ~450 ºCday range of GDD values. This means at Rosalia the GDD is not driving the vegetation onset, and this site is unlikely to be temperature-driven.

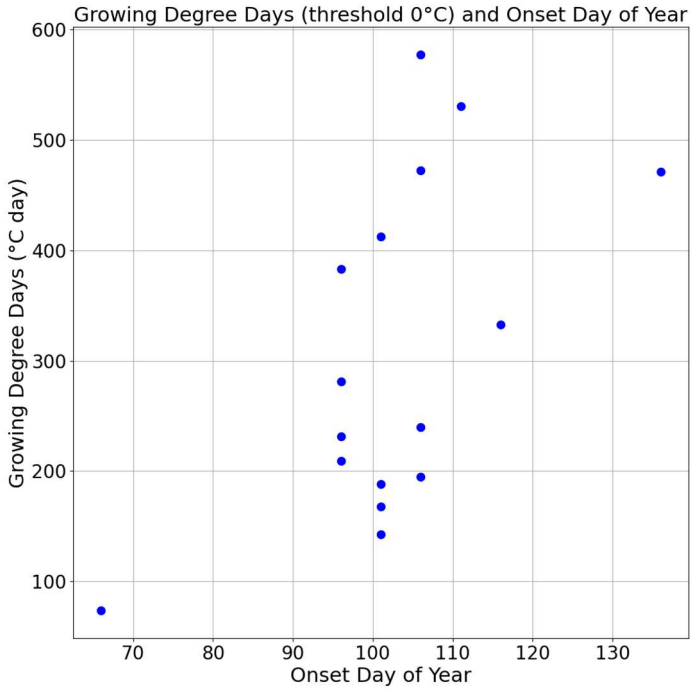

Figure 11: A comparison of the day of the year of vegetation onset and the accumulated growing degree days on that day, at the Rosalia site.

Figure 12: The day of the year of onset (green) and the day of the year the growing degree day value reaches a set accumulation with a temperature threshold of 0ºC (blue) at the Monte Bondone grass site. (top) The temperature accumulation is 150 ºC days. (bottom) The GDD temperature accumulation is 300 ºC days.

The two distinct modes of GDD-onset behaviour at Monte Bondone seen in Figure 10 are further explored by looking at the time series of these data. A second GDD calculation is performed to determine when the cumulative GDD first exceeds a specified accumulation. This date varies depending on the temperature threshold value used. Figure 12 shows the comparison between this GDD-based date (using a 0ºC threshold) and the onset date derived from CCI_LAI.

Two contrasting behaviours in these dates are seen at Monte Bondone. For the 150 ºCday threshold, the date GDD exceeds this level occurs within 15 days of the onset date during the years 2002-2009. Fifteen days is three timesteps in the CCI_LAI data; this is a strength of the CCI_LAI data that it can resolve these differences. After 2010, the two dates diverged from each other, with only 2018 having similar dates for the two events. Setting the GDD level to 300 ºCday brings the onset and GDD exceedance date back closer together in the later years, but to the detriment of increasing the difference between them in the early period. These time series patterns complement the bimodal patterns seen in Figure 10.

The trend in the date GDD exceeds the thresholds at Monte Bondone is not matched by the CCI_LAI-derived onset dates. This means that at this site it might not be possible to give a single set of criteria to determine if the vegetation phenology is temperature driven. The earlier GDD exceedance dates are indicative of increasing temperatures because of climate change. The vegetation at Monte Bondone may not have been able to adapt to this warming on these time scales. This observation gives the possibility of GDD being used to identify the effects of climate change and where the vegetation phenology is or is not changing on the same time scale.

4.3 Soil moisture-driven case: Savannah

The grass site for this case study is located in a Savannah biome (14.5°N 22°E), falls in the water-driven area, and shares the same plant type as Monte Bondone (Natural Grasses, GRASS-NAT). This site provides, therefore, a case study for estimating the relationship between SM and CCI_LAI. As it can be observed in Figure 13, the seasonal variability of CCI_LAI strictly resembles and follows the amount of volumetric Soil Moisture, with annual CCI_LAI peak almost exactly coinciding with the wettest days of the year, as a demonstration of the strong control of water availability on vegetation dynamics in semiarid and arid grassland ecosystems.

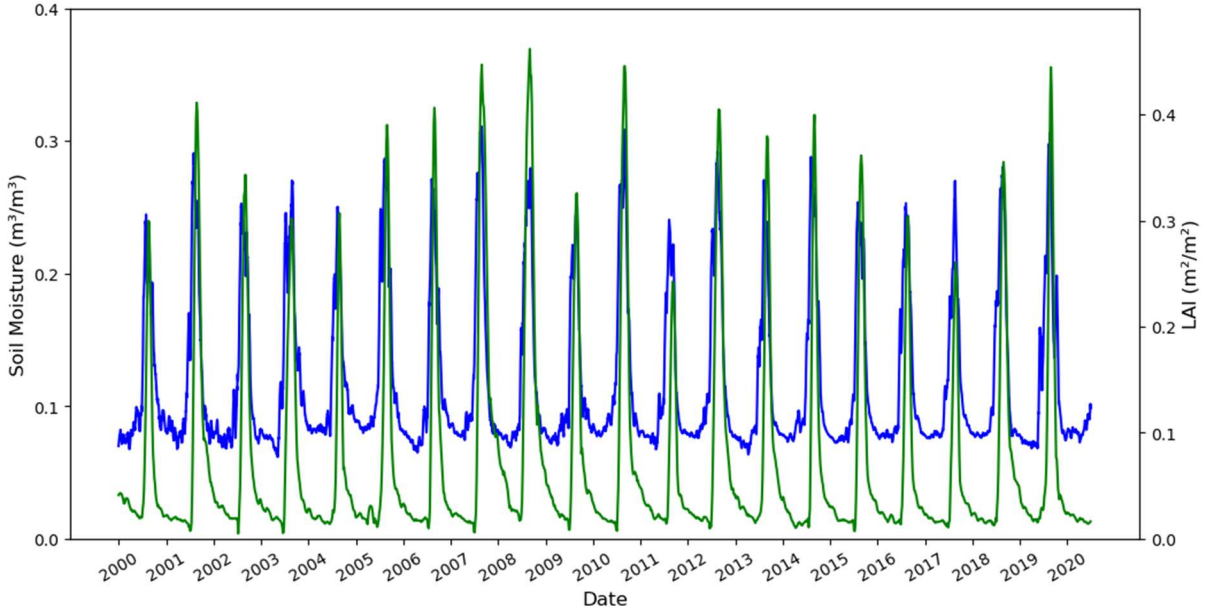

Figure 13: The soil moisture (blue) and CCI Leaf Area Index (CCI_LAI) (green) for the Savannah site in Chad (14.5°N - 22°E). There is a close alignment between the dates of the peak in soil moisture and the dates from the peaks in CCI_LAI.

The onset of the growing season is then computed from CCI_LAI and SM by applying 4GST and the approach presented in Section 3.3, respectively (Figure 14).

The comparison displays the phenology onset day of the year as predicted by both CCI_LAI 4GST algorithm (green line) and the SASM algorithm (brown dotted line) from 2000 until 2019. Overall, the LAI onset trend along the years is well captured by the soil moisture-based algorithm, with a Pearson correlation of 0.6, demonstrating the potential of using soil moisture data to successfully predict vegetation onset at this site. Additionally, the day of the year of phenology onset from CCI_LAI is precisely predicted for a good share of years, and depicts a maximum onset difference in the two estimation methods of 10 days, which is the equivalent of two timesteps for CCI_LAI dataset. Please note that the onset computation with the SASM algorithm has a daily timestep precision, which could itself explain part of the observed mismatch in Figure 14 compared to 4GST, which relies on 5 days CCI_LAI precision.

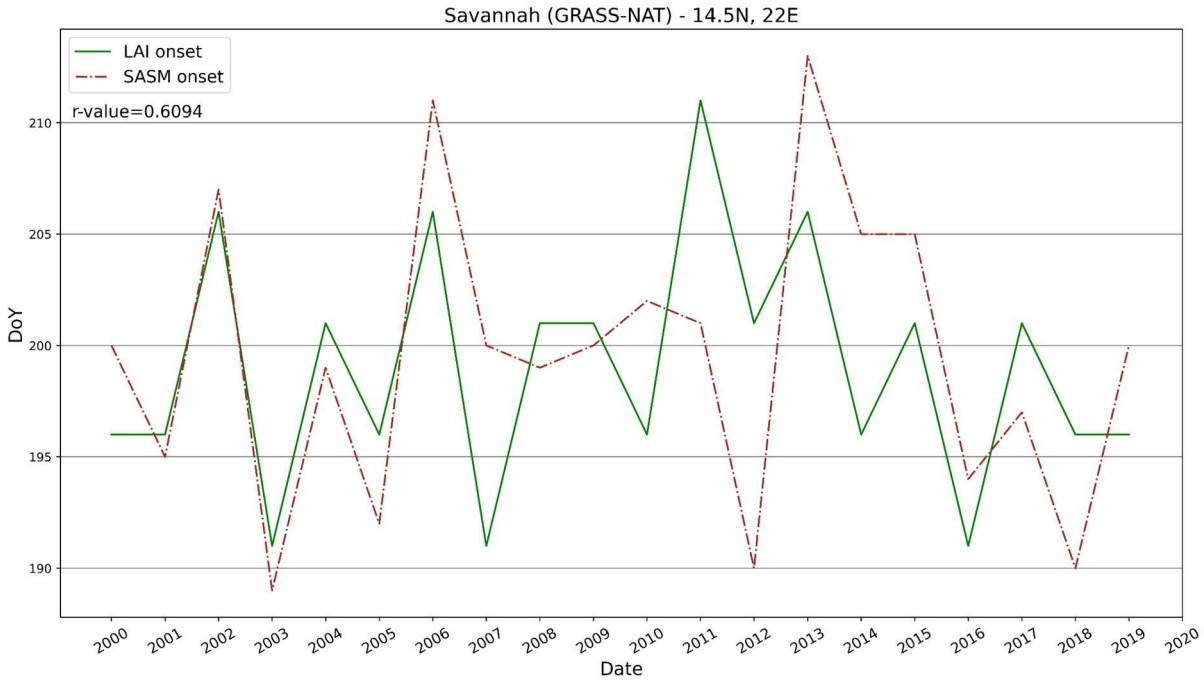

Figure 14: Comparison of vegetation onset dates derived from CCI Leaf Area Index (CCI_LAI) (green) and from the Standardized Amount of volumetric Soil Moisture (SASM method) (brown) at a savannah site in Chad.

5. Conclusions

The WP5.2 study provided a valuable collaboration between the CCI_LAI data developers (Vegetation CCI team) and its users (WP5.2 CMUG team), coinciding with the release of the

first version of CCI_LAI dataset. This timeline enabled a productive exchange of feedback and suggestions between the two teams throughout the study.

The approach of section 3.1 provides a method for processing the CCI_LAI data. Four stages are presented to clean the data by removing anomalous points, both that have a higher uncertainty by filtering using the CCI_LAI standard error, and those that are not in keeping with the wider time series by using *z*-scores. Filtering the dataset with both of these steps leaves a time series with several gaps. These gaps were filled using linear regression. A final stage applied a Savitzky-Golay filter to return a smooth time series that could be used for calculating phenology metrics.

The need for this data processing step highlights the challenges that users may encounter when working with the CCI_LAI data in its current form, version 1. There is currently limited knowledge of post-processing techniques for smoothing and gap-filling satellite data in the dataset documentation. A key outcome of this study is the request to the CCI Vegetation team, which can be extended to all CCI data producers, to provide examples, tools, or documentation on suitable data processing methods to support their users in applying the datasets effectively.

WP5.2 also stresses the connection between soil moisture, land surface temperature and plant phenology, represented by Leaf Area Index. Section 3.3 proposes and Section 4 explores a set of criteria to identify the main phenology driver, temperature or soil moisture, and the relationships between them and CCI_LAI.

In sites that are potentially temperature-driven, the GDD values are calculated from MW LST observations. The case study site at Monte Bondone shows a change in the relationship between onset derived from CCI_LAI and the dates GDD reaches a set accumulation. The example given at Rosalisa shows a contrasting behaviour where there is one relationship where vegetation onsite does not vary with GDD values. This shows GDD vs onset behaviour has the potential to identify different land cover types, and that its use in the criteria to define temperature-driven phenology needs further refinement.

The presence of the trend in GDD implies that a single set of criteria to apply across the whole time series to determine if a region is temperature driven might not be appropriate. It may be a better approach to investigate if individual years are temperature driven. This could give rise to indicators based on the early part of the year that will predict if the rest of the year will be, or become, temperature driven. Understanding how trends in GDD are related to the vegetation onset dates could be used to understand the impact of a warming climate on the vegetation and identify regions where the vegetation is not adapting to this change.

At the soil moisture driven case study site, the savannah site in Chad, the SASM method was used to identify the vegetation onset date. For the whole study period, 2000-2019, a good agreement was found between the onset date derived from soil moisture and the onset date derived from CCI_LAI. In regions with similar climatological conditions and vegetation characteristics, such as this site in the Sahel, the vegetation growth is tightly coupled to increases in soil moisture resulting from infrequent rainfall events, where plants quickly react to moisture availability. The close alignment between CCI_LAI-derived and SASM-derived phenological onset dates further supports this relationship, indicating that both approaches

capture the same underlying ecohydrological processes. Therefore, this consistency suggests that the two methods can be used complementarily, making SASM-derived onset as a reliable proxy for identifying vegetation phenology dynamics across semi-arid environments and water limited climatological regions.

After identifying whether a region's vegetation is temperature or moisture driven, the appropriate approach (i.e. GDD and SASM in temperature and water-limited regions, respectively) can be used to compute the start of the growing season. As seen in the Monte Bondone case study, trends in LST can be detected with GDD. The proposed relationships can be employed as indicators to evaluate LSMs or new approaches to compute phenophases within LSMs. This means that multiple variables can be used to evaluate the vegetation related predictions from LSMs, and not have to rely on just one quantity. Similarly, the relationship identified for the water-limited specific case study, can be upscaled and tested in the context of LSMs, potentially representing a way to better capture the phenology onset in complex process-based models.

However, these results are inherently limited by their derivation from a set of site-specific case studies. The identified relationships will be expanded to biomes or climate categories to enable a comparison with Earth System Models and extend the present results. This will be the focus of the OWP5.2 study within the CMUG framework. Besides, further investigation of the relationship between vegetation and hydrometeorological variables will be the focus of the OWP5.9 study.

6. References

Anon. (1969) Tables for the evaluation of daily values of accumulated temperature above and below 42°F from daily values. Met Office Leaflet, Number 10.

Baker, C.R.B (1980) Some problems in using meteorological data to forecast the timing of insect life cycles, EPPO Bull., 10 (2), 83-91.

Baret, F., Weiss, M., Lacaze, R., Camacho, F., Makhmara, H., Pacholcyzk, P., and B. Smets. (2013) GEOV1: LAI and FAPAR essential climate variables and FCOVER global time series capitalizing over existing products. Part 1: Principles of development and production, Remote Sensing of Environment, 137, 299–309, https://doi.org/10.1016/j.rse.2012.12.027.

Blessing, S. (2024). *CCI Vegetation Algorithm Theoretical Basis Document*.

Blunden, J. and T. Boyer, Eds. (2024) "State of the Climate in 2023". Bull. Amer. Meteor. Soc., 105 (8), Si–S484 https://doi.org/10.1175/2024BAMS State of the Climate. 1.

Harris, B.L., Taylor, C.M., Dorigo, W., Zotta, R.M., Ghent, D. and Noguera, I., 2025. Global observations of land-atmosphere interactions during flash drought. *EGUsphere*, *2025*, pp.1-24.

Clark, D. B., Mercado, L. M., Sitch, S., Jones, C. D., Gedney, N., Best, M. J., Pryor, M., Rooney, G. G., Essery, R. L. H., Blyth, E., Boucher, O., Harding, R. J., Huntingford, C., and Cox, P. M. (2011). The

Joint UK Land Environment Simulator (JULES), model description – Part 2: Carbon fluxes and vegetation dynamics, Geosci. Model Dev., 4, 701–722, https://doi.org/10.5194/gmd-4-701-2011.

Good, E. J. (2016), An in situ-based analysis of the relationship between land surface "skin" and screen-level air temperatures, J. Geophys. Res. Atmos., 121, 8801–8819, doi:10.1002/2016JD025318.

Good, Stephen P., Georgianne W. Moore, and Diego G. Miralles. "A mesic maximum in biological water use demarcates biome sensitivity to aridity shifts." *Nature ecology & evolution* 1, no. 12 (2017): 1883-1888. https://www.nature.com/articles/s41559-017-0371-8

Harris, B. L., Taylor, C. M., Dorigo, W., Zotta, R. M., Ghent, D., & Noguera, I. (2025). Global observations of land-atmosphere interactions during flash drought. EGUsphere, 2025, 1-24. https://doi.org/10.5194/egusphere-2025-1489

Lawrence, D. M., Fisher, R. A., Koven, C. D., Oleson, K. W., Swenson, S. C., Bonan, G., Collier, N., Ghimire, B., van Kampenhout, L., Kennedy, D., and 46 others. (2019) The Community Land Model version 5: Description of new features, benchmarking, and impact of forcing uncertainty, Journal of Advances in Modeling Earth Systems, 11, 4245–4287, https://doi.org/10.1029/2018MS001583.

Li, W., N. MacBean, P. Ciais, P. Defourny, C. Lamarche, S. Bontemps, R. A. Houghton, and S. Peng. (2018) Gross and net land cover changes in the main plant functional types derived from the annual ESA CCI land cover maps (1992–2015), Earth System Science Data, 10, 219–234, https://doi.org/10.5194/essd-10-219-2018.

Li, X., Melaas, E., Carrillo, C. M., Ault, T., Richardson, A. D., Lawrence, P., Friedl, M. A., Seyednasrollah, B., Lawrence, D. M., and A. M. Young. (2022) A comparison of land surface phenology in the Northern Hemisphere derived from satellite remote sensing and the Community Land Model, Journal of Hydrometeorology, 23(6), 859–873, https://doi.org/10.1175/JHM-D-21-0169.1.

Murray-Tortarolo, G., Anav, A., Friedlingstein, P., Sitch, S., Piao, S., Zhu, Z., Poulter, B., Zaehle, S., Ahlström, A., Lomas, M., Levis, S., Viovy, N., and Zeng, N. (2013) Evaluation of land surface models in reproducing satellite-derived LAI over the high-latitude northern hemisphere. Part I: uncoupled DGVMs, Remote Sens., 5, 4819–4838, https://doi.org/10.3390/rs5104819.

Peano, D., Materia, S., Collalti, A., Alessandri, A., Anav, A., Bombelli, A., and S. Gualdi. (2019) Global variability of simulated and observed vegetation growing season, J. Geophys. Res.-Biogeo., 124, 3569–3587, https://doi.org/10.1029/2018JG004881.

Peano, D., Hemming, D., Materia, S., Delire, C., Fan, Y., Joetzjer, E., Lee, H., Nabel, J. E. M. S., Park, T., Peylin, P., Wårlind, D., Wiltshire, A., and S. Zaehle. (2021) Plant phenology evaluation of CRESCENDO land surface models – Part 1: Start and end of the growing season, Biogeosciences, 18, 2405–2428, https://doi.org/10.5194/bg-18-2405-2021.

Peano, D., Hemming, D., Delire, C., Fan, Y., Lee, H., Materia, S., Nabel, J. E. M. S., Park, T., Wårlind, D., Wiltshire, A., and S. Zaehle. (2025) Plant phenology evaluation of CRESCENDO land surface models. Part II: Trough, peak, and amplitude of growing season, EGUsphere [preprint], https://doi.org/10.5194/egusphere-2024-4114.

Richardson A.D. (2023). PHENO CAM: an evolving, open-source tool to study the temporal and spatial variability of ecosystem-scale phenology. Agricultural and Forest Meteorology 342: 109751.

Swinnen, E., Vanhoof, K., Sanchez, J., Blessing, S., and C. Van der Tol. (2023) CCI+ Vegetation Parameters Product User Guide CRDP-1, 53 p., https://climate.esa.int/media/documents/VP-CCI_D4.2_PUG_V1.2.pdf.

Verger, A., Baret, F., Weiss, M., Filella, I., and Peñuelas, J. (2015) GEOCLIM: A global climatology of LAI, FAPAR, and FCOVER from VEGETATION observations for 1999-2010. Remote Sensing of Environment 166:126-137.

Verger, A., Lacaze, R., and Cherlet, M. (2019) Copernicus Global Land Operations "Vegetation and Energy" Algorithm Theoretical Basis Document - Leaf Area Index https://land.copernicus.eu/en/technical-library/algorithm-theoretical-basis-document-leaf-area-index-version-2/

White, M.A., Thornton, P.E., and S.W. Running. (1997) A continental phenology model for monitoring vegetation responses to interannual climatic variability. Global Biogeochemical Cycles 11:217-234.

Wolters, E. C. Toté, W. Dierckx, M. Paepen and E. Swinnen. (2023) PROBA-V Collection 2 Products User Manual v1.0, 78 p. https://probav.vgt.vito.be/sites/probavvgt/files/downloads/PROBAV_C2_Products_User_Manual.pdf.

Woodward (1987) Climate and Plant Distribution. Cambridge University Press.

7. Glossary

Terms	
Onset	The beginning of the growing season.
Offset	The end of the growing season.
Acronyms	
4GST	Four Growing Season Types
AMSR2	Advanced Microwave Scanning Radiometer - 2
AMSR-E	Advanced Microwave Scanning Radiometer for EOS
CCI	Climate Change Initiative
CMUG	Climate Modelling Users Group
ECV	Essential Climate Variable
GCC	Green Chromatic Coordinate
GDD	Growing Degree Day
IR	Infrared
LAI	Leaf Area Index
LSM	Land Surface Model
LST	Land Surface Temperature
MODIS	Moderate-Resolution Imaging Spectro-radiometer
MW	MicroWave

.

PFT	Plant Functional Type
PUG	Product User Guide
SASM	Standardized Amount of volumetric Soil Moisture
SM	Soil Moisture
SSM/I	Special Sensor Microwave Imager
SSMIS	Special Sensor Microwave Imager/Sounder
SWE	Snow Water Equivalent